Casimir force in micro and nano electro mechanical systems

Ricardo Decca[(1)], Vladimir Aksyuk[(2)] and Daniel López[(3)]

1. Indiana University-Purdue University Indianapolis
402 N. Blackford St, Room LD154; Indianapolis, IN 46202

2. Center for Nanoscale Science and Technology,
National Institute of Standards and Technology
100 Bureau Drive, MS 6203, Gaithersburg, MD 20899

3. Argonne National Laboratory, Center for Nanoscale Materials
9700 South Cass Avenue, Lemont, IL 60439

Abstract

The last 10 years have seen the emergence of micro- and nanomechanical force sensors capable of measuring the Casimir interaction with great accuracy and precision. These measurements have proved fundamental to further develop the understanding of vacuum fluctuations in the presence of boundary conditions. These micromechanical sensors have also allowed to quantify the influence of materials properties, sample geometry and unwanted interactions over the measurement of the Casimir force. In this review we describe the benefits of using micro-mechanical sensors to detect the Casimir interaction, we summarize the most recent experimental results and we suggest potential optomechanical experiments that would allow measuring this force in regimes that are currently unreachable.

Introduction

During the last 60 years, there have been considerable studies trying to understand the forces acting between electrically neutral objects in vacuum, particularly, the van der Waals and Casimir forces. The experimental characterization and physical interpretation of these interactions is still generating discussions and stimulating the development of increasingly sophisticated experiments.

In the late 1940s, Hendrik Casimir [1] demonstrated theoretically that there is an *attractive* force between two electrically neutral, perfectly reflecting, and parallel conducting plates placed in vacuum. This attractive force is known as the Casimir force and is considered a quantum phenomenon since in classical electrodynamics the force acting between neutral planes is strictly zero. Casimir compared the quantum fluctuations of the electromagnetic field existing inside and outside these ideal parallel plates. The plates impose well-defined boundary conditions to the fluctuating electromagnetic modes existing between them and, as a consequence, the zero-point energy of this system is a function of the separation between plates (see Figure 1). The difference between zero-point energy inside and outside the plates is responsible for the attractive force between plates. This force has the same origin as the van der Waals force but acts at larger separations between bodies and, as a consequence, relativistic retardation effects need to be considered.

According to Casimir's original calculation, the attractive force per unit area, i.e., the pressure between the plates, can be expressed as:

$$P\ d\ = -\frac{\pi^2 \hbar c}{240 d^4} \qquad (1)$$

where d is the separation between plates, c is the speed of light and $\hbar$ is Planck's constant divided by 2π. The calculation of the Casimir's pressure for dielectric surfaces at finite temperature was obtained by Lifshitz [2] in 1956. Several excellent reviews describing the theoretical aspects of these calculations and alternative derivations are listed in the reference section [3-15].

The simple Casimir formulation of the pressure acting between two neutral metallic plates represented one of the first indications that the zero-point energy of the electromagnetic field could be experimentally detected. The physical reality of the Casimir effect was a very controversial subject when proposed for first time. In his biography [16], Casimir described the unsuccessful discussions he had with Wolfgang Pauli trying to convince him that this force could have observable effects. Since then, there have been so many experimental confirmations of this force that its effects are now routinely considered when studying objects at separations below 1 μm.

The first experiment intended to measure the Casimir force was performed in 1958 by Sparnaay [17] using parallel plates. While this experiment was not very successful due to the difficulties associated with moving parallel plates with high precision, it provided the first indication that surface roughness needs to be reduced and surface charges must be removed. Blokland and Overbeek did the first convincing measurement of the Casimir force in 1978 [18]. By using a sphere in front of a metallic plate, to eliminate the problems associated with the parallelism of the plates, they measured the force with an experimental accuracy of 50%. The experiment done by S. Lamoreaux in 1997 [19] is considered the first high-precision measurement of the Casimir force. He used a torsional pendulum in the sphere-plate configuration and

obtained a 5% agreement between theory and experiment. Several variations of these experiments have been performed in the following years producing compelling evidence that the Casimir effect can be observed in various experimental conditions. A common feature of these experiments is that they involved *macroscopic* objects: They measured the Casimir force among objects having typical dimensions of several cm and for separations between bodies of the order of microns.

The first measurement of the Casimir force between *microscopic* objects separated by 100's of nanometers or less, was performed by Mohideen in 1998 [20] using an atomic force microscope (AFM). In this experiment, a gold-coated 200 μm diameter sphere was attached to the tip of an AFM, which was used to measure the Casimir force between the sphere and a metalized plate. Similar experiments using AFM techniques are very popular today since they allow the measurement of this force at distances as short as 20 nm [21].

The use of micro-mechanical devices as a novel technique for characterization of this force was introduced by Ho Bun Chan and collaborators at Bell Laboratories in 2001 [22]. In this technique, a micro-mechanical torsional oscillator is used to detect the Casimir force induced by a metallic sphere approaching the oscillator. Furthermore, this experiment demonstrated that the Casimir force could be used to modify the mechanical state of microscopic devices introducing a novel mechanism for actuation at the micro- and nanoscale. Casimir force detectors based on micro-mechanical devices are currently the most sensitive devices to characterize this force [23].

The infographics shown in Figure 2 summarizes the typical dimensions of the objects used in Casimir experiments performed in the last decades. The area labeled "torsion balance" represents the *macroscopic* experiments performed with objects having tens of cm in size. The use of MEMS (Micro Electro Mechanical Systems) and AFM (Atomic Force Microscopy) technology, what we call *microscopic* experiments, allowed precise determination of the Casimir force down to 20 nm distances by involving objects with sizes below 1 mm.

In this review, we will describe the fundamentals of micro and nano electro mechanical devices (NEMS), we will explain the advantages they provide when used to detect the Casimir force and we will examine the most recent results obtained with this technology. We conclude this review with suggestions to improve the precision of micro/nano mechanical sensors to enable the investigation of the Casimir force in regimes that are currently not accessible.

Micro and Nano electro mechanical systems

Mechanical devices with typical dimensions in the order of tens of microns, known as MEMS (Micro Electro Mechanical Systems), are already having a pervasive presence in science and technology [24]. They are widely employed as sensors and actuators due to their fast response time, enhanced sensitivity to external perturbations and the possibility of high-density integration of multiple elements into a single chip. By further reducing the size of these MEMS devices, we enter the world of NEMS (Nano Electro Mechanical Systems). In this size regime, the resonance frequency of these nano-devices becomes extremely large (up to GHz) and their mechanical quality factor remains very high ($Q \approx 10^6$). This combination implies exceptionally high force sensitivities, ultra-low power consumption and access to non-linear response with small actuation

forces [25]. Furthermore, NEMS devices allow integration of even larger number of nano-mechanical devices into extremely small areas.

As force detectors, MEMS and NEMS have been successfully used in a diversity of applications since they can routinely detect piconewtons (10^{-12} N) and, under special experimental conditions, they can detect forces as small as zeptonewtons (10^{-21} N). MEMS/NEMS based force sensors have been used to measure forces between individual biomolecules [26], to explore quantum effects in mechanical objects [27,28], to detect single spins by magnetic resonance force microscopy [29] and to study force fluctuations between closely spaced bodies [30]. As we will see in the following section, MEMS devices have also enabled the most precise measurement of the Casimir interaction between metallic objects in vacuum [23].

This long list of examples is also an indication of how vulnerable these devices are to local forces and to what extent local forces are to be considered in the design of MEMS/NEMS devices. In the particular case of the Casimir force, its effects become important when the distance between neutral objects is in the order of hundreds of nanometers. Fabrication of mechanical devices with features of this size is becoming common nowadays. Recently, high-density arrays of NEMS mirrors with critical dimensions of about 100 nm have been fabricated to modulate deep ultraviolet radiation (DUV) for maskless lithography applications [31]. These NEMS mirrors are separated by 100 nm gaps and they are supported at the center by 100 nm wide elastic springs providing the mechanical restoring forces (see Figure 3). In the absence of electrostatic actuation, the Casimir force is the dominant interaction between these miniature objects and it needs to be taken into account in their design.

In the following section, we will describe the use of MEMS devices as force sensors for unambiguous detection of the Casimir interaction between metallic objects.

Experimental aspects on the determination of the Casimir interaction

A MEMS torsional oscillator is at the core of the experimental setup developed to measure the Casimir interaction between metallic bodies. The attractive force between two bodies can be measured by determining the changes induced in a MEMS oscillator due the Casimir interaction. These changes could be associated with either an induced displacement of the oscillator or a change of its natural resonance frequency due to the presence of the interaction between the two bodies. Beyond the requirement of a precise determination of the interaction itself, the separation between the two bodies also needs to be measured accurately and precisely.

Our experimental setup has allowed us to obtain the most sensitive experimental determination to date of the Casimir interaction between similar and dissimilar metals. The current system consists of a MEMS torsional oscillator and a metal-coated sphere and is capable of extremely precise control of their relative position (see Figure 4a). The MEMS oscillator and the sphere are independently coated with the materials under consideration. By approaching a coated sphere to one side of the coated torsional oscillator the attractive Casimir force induces a torque that rotates the MEMS device about the fixed supports. This rotation is detected by measuring the angular deflection of the plate as a function of the plate-sphere separation. Furthermore, these MEMS oscillators can be designed to concurrently have high resonance frequencies and large quality factor Q producing important improvements in sensitivity. This experimental

setup can be operated in both static and dynamic regimes. In the static regime the sphere is maintained at a fixed vertical position and the Casimir force is measured directly. In the dynamic regime, the vertical separation between the sphere and the plate is changed harmonically with time, leading to an improvement of the sensitivity.

The MEMS is mounted onto a piezo-driven *xyz* stage which, in turn, is mounted on a micrometer controlled *xy* stage. This combination allows positioning the metal-coated sphere over the metal-coated MEMS plate. The separation z_i between the sphere and the substrate is controlled by the vertical axis of the *xyz* stage. A two-color fiber interferometer-based closed-loop system is used to measure and control z_i.

Measurements of the Casimir interaction have been performed in two different configurations. In the first one, Fig. 4a, the polysilicon oscillator plate was coated with a thin adhesion layer (≈ 10 nm of either Cr or Ti) and subsequently a thick (≈ 200 nm) Au layer was evaporated. Similarly, the $R \approx 150$ mm sapphire sphere was coated with ≈ 10 nm Cr and ≈ 200 nm Au was thermally evaporated on it. The Au coating in both the plate and the sphere is thick enough to ensure that the Casimir interaction can be regarded as arising from solid Au bodies, which was checked by calculating the Casimir interaction between bodies for a multilayer system [32] and, more importantly, by measuring the interaction using a sphere with a thinner (≈180 nm) Au layer. No significant differences between both experimental runs were observed. The Au-coated sphere was glued with conductive silver epoxy to the sides of an Al-coated optical fiber that is part of an optical interferometer. In the second setup, Fig. 4b, the position of the sphere and the plate has been interchanged. This new configuration permits easier exchange of samples without modification of the fragile MEMS sensor.

When confronted with the measurement of small forces, the isolation of the detecting device from external vibrations is of supreme importance. Hence, using a MEMS torsional oscillator is preferable, since torsional oscillators are less sensitive to vibrations that couple with the motion of their center of mass. Further decoupling from external vibrations is achieved by mounting the rigid sample setup by soft springs to a vacuum chamber, which in turn is on top of a passive damping air table. The incorporation of magnetic damping, along all axes of motion, between the sample setup and the vacuum chamber reducing vibrations to a peak-to-peak amplitude $\Delta z_{pp} < 0.02$ nm for frequencies above 50 Hz. The small dimensions of the oscillator aids in improving its intrinsic quality factor and sensitivity [33]. The high quality Q of the oscillator, however, cannot be fully utilized in the presence of a dissipative medium. The effects of energy damping of the surrounding air are minimized by working in a vacuum. The vacuum is achieved by pumping the system down to $1.3\ 10^{-5}$ Pa (10^{-7} Torr) with an oil free diaphragm-turbomolecular pump system. While measurements are performed, pumping in the sample chamber is stopped and the pump is physically disconnected from the system. A low pressure (never higher than $1.3\ 10^{-3}$ Pa (10^{-5} Torr)) is maintained by a chemical pump made of a cold (≈ 77 K) activated carbon trap located inside the vacuum chamber.

In both experimental situations the optical fiber can be moved relatively to the oscillator assembly by means of a five-axis micrometer driven mechanical stage, and a *xyz* piezo-driven stage.

The separation dependent attractive force $F(z_{metal})$ between the sphere and the plate will cause the oscillator to rotate under the influence of the torque

$$\tau = bF(z_{metal}) = k_{torsion}\,\theta \qquad (2)$$

where $k_{torsion}$ is the torsional spring constant for the oscillator. Since the torsional angles are small, they are proportional to the change in capacitance between the underlying electrodes and the oscillator. Consequently,

$$\theta \propto \Delta C = C_{right} - C_{left} \qquad (3)$$

where C_{right} (C_{left}) is the capacitance between the right (left) electrode and the plate (Fig. 4). Hence the force between the two metallic surfaces separated by a distance z_{metal} is $F(z_{metal}) = k\Delta C$, where k is a proportionality constant that needs to be determined by calibration.

Alternatively, the force sensitivity of the oscillator can be enhanced by performing a dynamical measurement [22,34,35]. In this approach, the separation between the sphere and the MEMS oscillator plate is varied as $\Delta z = A\cos(\omega_{res}\, t)$, where ω_{res} is the resonant angular frequency of the oscillator, and A is the amplitude of motion. The linearized solution for the oscillatory motion, valid for $A << z_{metal}$, yields [22,34]

$$\omega_{res}^2 = \omega_o^2\left[1 - \frac{b^2}{I\omega_o^2}\frac{\partial F}{\partial z}\right], \qquad (4)$$

Where, for $Q >> 1$, $\omega_o \approx \sqrt{k_{torsion}/I}$ is the natural resonance frequency of the oscillator, I is its moment of inertia. It has been shown [36] that there is an optimal value of A which is a function of the separation. If A is too small, then the error in the determination of ω_{res} increases due to thermal motion. If A is too large, then non-linearities can not be neglected. In general, A is selected to be between 2 nm and 5 nm to satisfy the aforementioned constrains. The resonance frequency can also be measured by recording the thermal vibration of the oscillator at temperature T, but it was found that driving the system with a sinusoidal signal and a phase-lock loop [34] provided a more stable signal.

Unlike the static regime where forces are measured, in the dynamic regime the force gradient $\partial F/\partial z$ is measured by observing the change in the resonant frequency as the sphere-plate separation changes. When F is given by the Casimir interaction, the gradient of the interaction within the applicability range of the proximity force, is found to be

$$-\frac{\partial F_C}{\partial z} = 2\pi R\, P_C(z_{metal}) \qquad (5)$$

where $P_C(z)=(F_C/S)$ is the force per unit area between two infinite metallic plates at the same separation z_{metal} as the sphere and the plate. In (5) F_C has been used to denote the Casimir interaction.

Calibrations

The characterization of the system and the determination of the calibration constants are performed by applying a known electrostatic force between the sphere and the MEMS plate, i.e, by applying a known potential difference, V_b , between them. In this case, the electrostatic force can be approximated by the force between a sphere and an infinite plate [37]:

$$F_e(z_{metal},V) = -2\pi\varepsilon_o (V_b - V_o)^2 \sum_{n=1}^{\infty} \frac{\coth(u) - n\coth(nu)}{\sinh(nu)} \cong \Xi(z_{metal})(V_b - V_o)^2 \qquad (6)$$

$$\Xi(z_{metal}) = -2\pi\varepsilon_o \sum_{m=0}^{7} B_m t^{m-1} \qquad (7)$$

In Eqs. (6) and (7) ε_o is the permittivity of free space, V_o is a residual potential difference between the plate and the sphere, $u = 1 + t$, $t = z_{metal}/R$, and B_m are fitting coefficients. While the full expression (6) is exact, the series is slowly convergent, and it is easier to use the approximation developed in Refs. [38] and [39]. The values of the B_m parameters are 0.5, -1.18260, 22.2375, -571.366, 9592.45, -90200.5, 383084, and -300357. Using these values, errors smaller than 1 part in 10^5 are obtained. In (6) it has been assumed that the contact potential V_o is independent of separation. If this is not the case a more involved analysis where the $V_o(z_{metal})$ dependence is taken into account would be needed [40].

To complete the electrostatic calibration (as well as to perform the measurement of the separation dependence of the Casimir interaction) it is necessary to determine z_{metal}. This variable can be determined precisely by using the following geometrical relationship (see Fig. 4a):

$$z_{metal} = z_i - z_o - z_g - b\theta \qquad (8)$$

In equation (8), z_g is the distance between the top of the MEMS oscillator and the substrate. This distance is measured interferometrically with an error of $\delta z_g \approx 0.1$ nm. The distance b is measured optically ($\delta b \approx 2$ μm), θ is determined through the change in capacitance between the oscillator and the underlying electrodes ($\delta\theta \approx 10^{-7}$ rad) and z_i is measured with a two-color interferometer where the light reflected at the end of the fiber is combined with the light reflected at the reference platform. The two-color interferometer, which operates with a low coherence source (superluminescent diode, coherence length ≈ 20 μm) at 1310 nm and a stabilized laser at 1550 nm, is a fiber version of the one developed in Ref. [41]. The distance z_o is not known *a priori* and the electrostatic calibration is also used to determine it [42].

The electrostatic calibration is done at z_{metal} large enough such that the Casimir interaction does not have a measurable contribution. For a fixed $(V_b - V_o)$, z_i is measured. With the best estimate for z_o (optically measured with an error of ≈ 2 μm), an iterative method is then used. As a function of measured separations z_i, the change in capacitance between electrodes and the plate is found [35] and from here the corresponding values of θ are obtained. This is repeated for up to 150 different $(V_b - V_o)$. With the measured values of θ and the estimated value for z_o, a set of z_{metal} values is obtained from (8). Using

$$\theta = \frac{b}{k_{torsion}} \Xi (z_{metal} + \delta z_o)(V_b - V_o)^2 \qquad (9)$$

$k_{torsion}/b$ and δz_o are used as fitting parameters. The improved value of z_o is used in (7) and the procedure is repeated until no further changes are obtained. The sensitivity of this approach is shown in Fig. 5. When all the errors are combined, it is found that z_{metal} can be measured to within δz_{metal} = 0.6 nm [36].

The electrostatic interaction is also used to obtain b^2/I. Typically for the first configuration (sphere on the fiber) $b^2/I \approx (1.2500 \pm 0.0005)$ mg^{-1}. When the sphere is attached to the oscillator the values of b^2/I are reduced by up to an order of magnitude (and vary significantly depending where the sphere is attached).

Once the electrostatic force has been used to calibrate the system, selecting $V_b = V_o$ makes the effect of the electrostatic interaction undetectable in our experiment. This is accomplished by applying a potential difference between the sphere and the plate $V_b = V_{DC} + \delta V \cos(\omega t)$, where the amplitude of the oscillatory component $\delta V \approx 1$ mV. The response of the oscillator is then proportional to $\partial F_e / \partial V_{DC}$, and V_o is obtained when the derivative of the force equals 0, as shown in Fig. 6.

Determination of the Casimir interaction

Upon completion of the calibration procedure, the Casimir interaction can be determined. The electrical potential between the sphere and the plate is adjusted as to obtain a null F_e, $V_b = \langle V_o \rangle$, where $\langle V_o \rangle$ is the average potential for z_{metal} in the 160 nm to 5000 nm range, found as described in the previous section. The position of the fiber is then changed in ≈ 2 nm increments, as measured by the two color interferometer. The actual z_{metal} is obtained using Eq. (8) with previous determination of the corresponding θ. The resonance frequency of the oscillator is measured, and by means of Eq. (5), the equivalent Casimir pressure $P_C(z_{metal})$ is obtained. The procedure is repeated for many runs (where the measurements are performed at the same set of z_{metal} within the experimental error) and the average of the different runs is reported as $P_C(z_{metal})$. When taking into account the errors in the determination of ω_{res}, $\delta\omega_{res} \approx 5$ mHz, and R, $\delta R \approx 0.3$ μm as determined in a scanning electron microscope, the total error in P_C can be determined [36,43]. Figure 7 shows the determination of P_C obtained by both experimental setups, with the sphere attached either to the fiber or to the sensor. Also in Fig. 7 the difference between both determinations is plotted. It is worth mentioning that these experiments were done with a separation of four years, in different vacuum chambers, using different experimental setups, and, more important, with Au deposited by different techniques. The data reported in Fig. 7 represent the most precise measurements of the Casimir interaction up to date. The error bars represent the 95 % confidence level in both the separation and pressure determination.

The characterization of the frequency dependence of the dielectric function $\varepsilon(\omega)$ of the material is required in order to calculate the Casimir force between real metals. Figure 8 shows our experimental measurements of the real, ε', and imaginary ε'' parts of the dielectric function of the Au layer deposited on a Si single crystal. The measurements were performed between 196 nm and 820 nm. While there are differences between the values measured on our samples and the ones reported on standard reference books [45],

it is important to notice that these differences are too small to produce any significant difference in [46] the calculation of the Casimir interaction [32].
In fact, the calculation of the Casimir pressure at finite temperatures for real samples is given by the Lifshitz formula [2,47]

$$P_C(z_{metal}) = -\frac{k_B T}{\pi} \sum_{l=0}^{\infty}{}' \int_0^{\infty} k_\perp dk_\perp q_l \times \left\{ r_{||}^{-2}(\xi_l, k_\perp) e^{2q_l z} - 1]^{-1} + [r_\perp^{-2}(\xi_l, k_\perp) e^{2q_l z} - 1]^{-1} \right\} \quad (10)$$

where $\boldsymbol{k}_\perp$ is the wave vector component in the plane of the plates, $q_l^2 = k^2{}_\perp + \xi_l^2/c^2$, $\xi_l = (k_B T l)h^{-1}$ are the Matsubara frequencies, and $r_{||}$ and $r_\perp$ are the reflection coefficients for two independent polarization states computed for imaginary frequencies $\omega_l = i\,\xi_l$. The prime on the summation in Eq. (10) refers to the inclusion of a factor ½ for the term with $l = 0$.

As described in the Refs. [36] and [43], the roughness of the sample also needs to be taken into account. By using the atomic force microscope image of the surfaces the fraction of the sample a different absolute separations are determined. The Casimir pressure between the two surfaces is obtained as the weighted average (weighted by the fraction of the sample at a given separation) of the Casimir pressure between samples of finite conductivity and at finite temperatures as given by Eq. (10). When the dielectric function is used in (10), different results are obtained when the zero order term of the Matsubara series is computed using a Drude model or a plasma model. A detailed discussion of the comparisons can be found in Refs. [36], [43] and [48]. Here it suffices to include the obtained results as a function of separation, as shown in Fig. 9. While the plasma model shows an excellent agreement with the data, no agreement within the experimental error is obtained when the Drude model is used. This remarkable result is still waiting for explanation, and has given rise to numerous problems and controversies in the interpretation of the data.

Current discussions in the precise determination of the Casimir force

As aforementioned, the discrepancies between experiments and the Drude model have resulted in numerous controversies. It is difficult to understand why while the low frequency transport of Au is very well described with a Drude model, the effects of dissipation on the conduction electrons are absent when performing Casimir pressure measurements. Among the arguments brought forward to explain these discrepancies, it has been hypothesized that differences in the Au layer could account for them. While this has not been completely ruled out, the data showed in Fig. 9 is a strong indication that this is not the case. Furthermore the effect of having a poor Au metallic coating would be to decrease the strength of the Casimir interaction, making the difference with the observed data more pronounced. In a recent experiment [44] we intended to provide an answer to this problem by measuring the Casimir pressure at different temperatures, ≈2 K, 4.2 K, 77 K and 300 K. The idea here was to find out if as the temperature was reduced the measured Casimir pressure remained constant (thus supporting the plasma model) or changed (as it would be the result expected when dissipation is reduced). Unfortunately, while the average of $P_C(z_{metal})$ remains the same at all temperatures, the data shows a significantly larger amount of noise at low temperatures precluding the

exclusion of either model. Other possibilities that have been mentioned is the existence of a systematic effect associated with either an improper electrostatic calibration, or the presence of patch potentials that provide an extra attractive interaction.

Additionally, there has been some controversy regarding the electrostatic calibration of the experimental setup. Particularly, the dependence of V_o between metallic layers has been significantly studied as a function of position, separation, and time. Differently from what other groups have found [40], in our samples V_o was observed to be independent of time, position or separation, as shown in Fig. 10, in agreement with what has been reported on Ref. [39]. Alternatively, there is an experimental report indicating that an electrostatic calibration free of the problems can be obtained even when V_o changes with separation [49]. While the results obtained by our group are in good agreement with theoretical expectations, the reasons behind the different observations in different configurations require further study. This dependence could be associated with patch potentials, which would yield a separation dependence of V_o and a residual electrostatic force that cannot be counterbalanced [50,51]. In Ref. [36] it was calculated that the effect of patch potentials would be undetectable if their extent were to be ≈ 300 nm (estimated Au grain size in the samples). If, on the other hand, the patches are very large, much larger than the effective interacting area, then their effect also would be cancelled by the effect of the applied V_b.

Finally, to shed more light on the effect of V_o on the interaction measurements, an experiment was performed where the applied V_b did not completely cancel V_o, leading to an effective "residual potential." The Casimir pressure was determined for this situation and when the optimal V_b was applied, and their difference plotted as a function of separation, as shown in Fig. 11. It is worth mentioning that firstly, a "residual potential" larger than the error in the average of V_o is needed to observe any effect in the interaction. Secondly, the interaction associated with the residual potential is well fitted by Eq. (6) with a leading $1/z_{metal}^2$ term at small separations. It appears from the totality of electrostatic measurements performed that the effects of residual potentials can be counterbalanced in the precision measurements of the Casimir interaction.

Future directions: improved micromechanical force sensors.

Investigations of the Casimir interaction stand to benefit considerably from the ongoing improvement in the precision micromechanical sensors and the associated position and force measurement techniques. The precision of the current generation of micromechanical sensors is significantly limited by the combination of the thermal noise of the mechanical sensor itself and the readout noise of the electrostatic or optical detector used in the MEMS or AFM based sensors respectively. In the case of MEMS sensors in particular, the Casimir force measurement precision has benefitted considerably from the stabilization of the measurement apparatus enabling very long acquisition times to improve the signal to noise ratio by signal averaging. It is however still desirable to improve the force and displacement measurement precision of these devices. This would enable the investigation of Casimir force in the regimes that were not previously easily accessible.

In the regime of large separation distance the Casimir force and its gradient are very weak and better force sensitivity would lead to an immediate improvement in that regime. In the regime of small separation distances the current limitation is the stability

of the sensor against the destabilizing effect of the Casimir force gradient – negative "Casimir spring" – leading to inability to maintain controlled constant separation. This can be counteracted by oscillating the mechanical sensor with large amplitude and essentially sampling the Casimir force at small separations only over a short portion of the oscillation cycle. This however leads to stringent oscillation amplitude control and measurement requirement, as well as a nontrivial relationship between the Casimir potential, oscillation amplitude and the measured oscillation frequency shift. A more straightforward way to access this regime is to increase the stiffness of the mechanical sensor to maintain its stability. However combining the stiffer micromechanical sensor (lower mechanical gain) with the decreased oscillation amplitude needed to maintain a simple linear measurement leads to a significant reduction in the signal to noise that need to be compensated for.

Finally, there is a significant recent interest in measuring the forces acting on objects that are spatially finite and have micron or even submicron dimensions, in order to observe size and shape dependence of the Casimir forces as well as potentially spatially inhomogeneous electrostatic forces due to so-called "patch potentials". To realize such measurements, again, dramatic improvements in sensor precision are required.

In considering the force measurement by a mechanical sensor we need to essentially consider two transduction or "amplification" stages. The first one is mechanical, whereby a mechanical force is transduced to a displacement of a linear mechanical oscillator. It is characterized by stiffness (gain), effective mass or resonance frequency, and mechanical loss (with the corresponding thermal noise). In the second stage the mechanical displacement is transduced into an electrical signal, typically through either an electrostatic or an optical measurement. This stage can also be characterized by its gain and the input referred noise. In an ideal case the gains are such that the noise of the first stage is dominant at all frequencies, but this is typically not the case.

In the first stage the mechanical loss essentially couples the oscillator to a thermal bath and introduces a mechanical thermal noise. The input-referred force noise spectrum of this Langevin force is white, independent of the frequency of the measurement. Consequently if the mechanical thermal noise of the transducer is the dominant noise source, the signal-to-noise (SNR) ratio of the measurement is also uniform and independent of frequency. The SNR is however inversely proportional to the square root of the loss, that is proportional to the square root of the mechanical quality factor Q. Note that when we measure the force at frequencies below the mechanical resonance frequency, the gain of the sensor is independent of Q, while the mechanical force and displacement noises decrease as $Q^{1/2}$. On the other hand, when we measure on resonance, the gain increases as Q, the force noise decreases as $Q^{1/2}$ and the corresponding displacement noise increases as $Q^{1/2}$. Thus the SNR improves with Q equally for off-resonance and on resonance measurement when thermal mechanical noise is dominant. When this is the case, SNR can only be improved by either increasing the force signal being measured, or by decreasing the equivalent temperature of the mechanical mode of the transducer during the measurement (see below).

In reality, however, there are technical and other noises, often referred to as 1/f noise, which can increase the noise floor at low frequencies above the thermal noise. In

addition, in most practical situations the gain of the mechanical transducer off-resonance is too low, resulting in electrical or optical noise of the second stage dominating everywhere except the narrow window around the mechanical resonance frequency. To take advantage of the high mechanical gain and high SNR around the mechanical resonance, the input force should be applied at the appropriate resonance frequency. With a force that is constant in time but that is a strong function of the separation gap this is achieved by modulating the gap. While the gap can be modulated by an external actuator, more often this is achieved by exciting the mechanical vibration of the transducer itself by applying an external force to it in parallel with the force to be measured. For example this force could be an electrostatic force, or an inertial force applied by vibrating the whole transducer in space.

Typically the measured transducer position is used in a phase locked loop to apply the external excitation force exactly at 90-degree phase shift to the measured transducer displacement while maintaining the constant transducer vibration amplitude. This insures that the transducer always vibrates on resonance. In turn the interaction force now has a component that is AC modulated by the oscillating transducer gap. For a potential force that is only a function of the gap, this AC component is in phase with the mechanical motion and results in the shift in the resonance frequency of the transducer, which is then being detected. For a small oscillation amplitude the measurement is particularly easy to interpret, as the frequency shift is proportional to the gradient of the force of interest at a given separation, see Eq. (4). However it should be noted that the AC force component that is being generated and measured in this way is almost always smaller than the total DC force at that gap. The SNR of this measurement is proportional to the vibration amplitude for small amplitudes.

In both DC and AC measurements the gain of the mechanical sensor is inversely proportional to the sensor stiffness. However, making the sensors softer leads to earlier onset of instability for small separations. Moreover, as long as the sensor effective mass is limited by the need for extended sensor position readout areas, such as the case for electrostatic readout, decreasing the sensor stiffness leads to lowering the resonance frequency. While dynamic measurement bandwidth is not a concern where a DC force is measured and the averaging time is seconds or even minutes, staying above the low frequency technical noise and maintaining high Q of the sensor prevents further reduction of the stiffness. The issues of the measurement bandwidth indeed come to the foreground as one considers scanning probe sensors where the force is measured as a function of location.

We can thus conclude that the DC and off-resonance force measurement SNR is currently limited directly by the mechanical displacement readout, while for on-resonance measurements with high Q transducers in vacuum thermal mechanical noise and the gap modulation amplitude determine the SNR at room temperature. Furthermore, decreasing the physical size of the position readout areas without compromising the readout precision would be required for more robust and higher bandwidth sensors.

While electrostatic readout has been widely used for MEMS sensors due to its relative simplicity of implementation in a MEMS transducer, it has significant limitations. It does not scale well with decreasing sensor size, as the capacitance derived signal is proportional to the area of the sensor. Even when the stray capacitance of the

cables connecting the sensor is eliminated, the input capacitance of the readout transistor, together with the electronic Johnson noise, limits this readout scheme.

Optical readout, however, has been shown to achieve much lower mechanical displacement noise levels, while requiring the minimum interaction areas only of the order of the wavelength of light used. The fundamental noise limit is in this case imposed by the quantum optical shot noise, and is generally independent of temperature as the energy of a photon in the visible to near-IR range of the spectrum is much larger than k_BT, where k_B is the Boltzmann's constant.

To realize the full benefit of the optical readout scheme one needs to use an optical interferometer that has as high finesse as possible and is modulated as strongly as possible by the mechanical motion of the sensor. In one recent example of a comparably low finesse (≈ 20) cavity using a gold-coated micromechanical cantilever as one of the mirrors, the mechanical noise level of the order of 10^{-15} m/Hz$^{1/2}$ was achieved [52] with incident optical power of 1mW and the readout spot on the cantilever of only 3 μm in size. In another remarkable example using a high finesse cavity (≈ 30000), spot size of ≈ 60 μm and incident power of 1.5 mW the noise level of $4\text{x}10^{-19}$ m/Hz$^{1/2}$ was achieved [53]. In both cases the optical cavities were of the order 1mm in size, external to the mechanical devices, and in the high finesse case the mechanical device was fairly large, 1mm x 1mm x 60μm, and included a high reflectivity coating.

The next step in the transducer evolution is to integrate the high finesse optical interferometer on the same chip, optomechanically coupled to the mechanical transducer for optical readout (and even possibly excitation with an all-optical force). The optical resonators with optical Q of over 10^5 and as small as a few microns in size can be realized on chip via appropriate microfabrication processes. Planar structures such as photonic crystals and disk and ring resonators are some of the possible candidates, combining compactness and high mode confinement with excellent Qs and the ability to integrate with connecting waveguides as well as mechanical sensors.

Such an integrated device coupling a MEMS transducer with an optical interferometer has been recently realized [54]. The concept is shown schematically in Figure 12. A high optical Q 10 μm diameter Si microdisk resonator is mechanically fixed to a substrate. The light can be coupled in and out of the resonator via a fixed microfabricated Si waveguide (WG) on a side of the resonator. A movable dielectric membrane (blue), made from low stress silicon nitride (LSN), is fabricated above the resonator. The membrane is attached to a MEMS transducer such as an electrostatic actuator and is capable of mechanical motion in the vertical direction. The optical mode in the microdisk is evanescently coupled to the membrane and as the membrane moves toward and away from the microdisk, never touching it mechanically, the motion significantly shifts the resonance frequency of the mode. While this is still work in progress, given the observed parameters of the current devices we estimate the shot noise limit of the mechanical motion readout to be below 10^{-15} m/Hz$^{1/2}$. With the evanescent field coupling approach the optical and mechanical devices are fabricated side by side and can be optimized essentially separately. No compromises are required such as integrating complicated and heavy coatings on micromechanical devices. Another advantage is the potential for completely fiber-pigtailed simplicity, without need for maintaining external optical alignment.

This type of device would in principle allow one to exploit various effects observed in cavity optomechanical systems [55]. One particular possibility is to excite the resonant vibration of the mechanical mode with an optical force by blue-detuning the optical excitation from resonance and use this as an alternative to the phase locked loop of the frequency sensing scheme described above. An even more exciting possibility is to use the position sensing for cooling the mechanical mode. This can be done either through feedback, or even directly by red-detuning the excitation light. For example, cooling factor of 60 from room temperature was achieved by using feedback approach [53]. While the cooling feedback is turned on, the effective mechanical Q is dramatically reduced, however as soon as the cooling is completed and the feedback is turned off, the Q is high and the thermal noise in sensor displacement is still low, while it takes the time of order Q/f_{res} for the mechanical mode to thermalize back to room temperature. If the cooling rate with the feedback turned on (in principle limited just by the opto-mechanical position sensing bandwidth and noise) can be made much faster than $1/Q$, the sensor can in principle be operated at the effective temperature much lower than room temperature.

Acknowledgments

R. S. D. acknowledges support from the National Science Foundation (NSF) through grants Nos. CCF-0508239 and PHY-0701236, Los Alamos National Laboratories (LANL) support through contract No. 49423-001-07. The authors are grateful to the Defense Advanced Research Projects Agency (DARPA) grant No. 09-Y557.

References

1. H. B. G. Casimir, “On the attraction between two perfectly conducting plates”, Proc. K. Ned. Akad. Wet. 60, 793 (1948).
2. E. M. Lifshitz, “The theory of molecular attractive forces between solids”, Sov. Phys. JETP, 2, 73 (1956).
3. P.W. Milonni, “The Quantum Vacuum: An introduction to Quantum Electrodynamics”; San Diego, CA: Academic, 1993.
4. M. Bordag, G. L. Klimchitskaya, U. Mohideen, V. M. Mostepanenko, “Advances in the Casimir effect”. Oxford University Press Inc., New York, 2009.
5. K. A. Milton, “The Casimir Effect: Physical Manifestations of Zero-point Energy”, Singapore: World Scientific, 2001.
6. V. M. Mostepanenko and N. N. Trunov, “The Casimir Effect and its applications”. Oxford, U.K.: Oxford University Press, 1997.
7. V. A. Parsegian, “Van der Waals forces: a Handbook for biologists, Chemists, Engineers and Physicist”. New York: Cambridge University Press, 2006.
8. L. Spruch, “Long range (Casimir) interactions”, Science 272, 145, 1996.
9. Daniel Kleppner, “With apologies to Casimir”, Physics Today, October 1990, page 9
10. Steve Lamoreaux, “Casimir forces: still surprising after 60 years”, Physics Today, February 2007.
11. R. L. Jaffe and A. Scardicchio, “Casimir effect and geometric optics,” Phys. Rev. Lett. 92, 070402, 2004.
12. A. Scardicchio and R. L. Jaffe, “ Casimir effect: an optical approach” Nucl. Phys. B. vol 704, 552, 2005.
13. Special issue, “Focus on Casimir forces,” New J. Phys. 8, October 2006
14. G. L. Klimchiskaya, U. Mohideen and V. M. Mostepanenko, “The Casimir force between real materials: experiment and theory”, Rev. Mod. Phys. 81, 1827, 2009.
15. F. Capasso, J. N. Munday, D. Iannuzzi and H. B. Chan, “Casimir forces and quantum electrodynamical torques: physics and nanomechanics”, IEEE J. Selected. Topics in Quantum Electronics 13, 400, 2007.
16. E. Elizalde, “A remembrance of Hendrik Casimir in the 60th anniversary of his discovery, with some basic considerations on the Casimir effect”, Journal of Physics: Conference Series 161, 012019, 2009.
17. M. J. Spaarnay, “Measurements of attractive forces between flat plates”, Physica, vol 24, 751, 1958.
18. P. H. G. M. van Blokland and J. T. G. Overbeek, “van der Waals forces between objects covered with a chromium layer”, J. Chem. Soc., Faraday Transactions 74, 2637, 1978.
19. S. K. Lamoreaux, “Demonstration of the Casimir Force in the 0.6 to 6μm Range”, Phys. Rev. Lett. 78, 5, 1997.
20. U. Mohideen and A. Roy, “Precision Measurement of the Casimir Force from 0.1 to 0.9μm*”,* Phys. Rev. Lett. 81, 4549, 1998.
21. T. Ederth, “Template-stripped gold surfaces with 0.4 nm rms roughness suitable for force measurements. Application to the Casimir force in the 20-100 nm range.” *Physical Review A* **62**, 62104 (2000).

22. H. Chan, V. A. Aksyuk, R. N. Kleiman, D. J. Bishop, and F. Capasso, "Quantum Mechanical Actuation of Microelectromechanical Systems by the Casimir Force," Science 291, 1942 (2001).
23. R. Decca. D. López, E. Fischbach, G. Klimchitskaya, D. Krause and V. Mostepanenko, "Precise Comparison of Theory and New Experiment for the Casimir Force Leads to Stronger Constraints on Thermal Quantum Effects and Long-range Interaction," Annals of Physics 318 (2005), 37.
24. Stephen Senturia, "Microsystems Design", Springer, NY, 2000.
25. K. Ekinci and M. Roukes, " Nanoelectromechanical systems", Rev. Sci. Instrum. **76**, 061101 (2005).
26. C. Bustamante et al., "Mechanical processes in biochemistry"; Annu. Rev. Biochem. 73, 705 (2004);
27. A. D. O'Connell et al., "Quantum ground state and single-phonon control of a mechanical resonator"; Nature **464**, 697, 2010.
28. K. Schwab and M. Roukes, "Putting mechanics into quantum mechanics"; Physics Today, July 2005, 36.
29. D. Rugar et al., "Single spin detection by magnetic resonance force microscopy", Nature 430, 329 (2004).
30. B. C. Stipe at al., "Noncontact friction and force fluctuations between closely spaced bodies"; Phys. Rev. Lett. 87, 096801 (2001).
31. D. López et al., "Two dimensional MEMS piston array for Deep UV optical Pattern generation"; Proc. IEEE/LEOS International Conf. on Optical MEMS and their applications, 148 (2006); V. Aksyuk et al., "MEMS spatial light modulator for optical maskless lithography"; Solid State Sensors, Actuators and Microsystems workshop, Hilton Hear 2006.
32. M. Bordag, U. Mohideen, and V. M. Mostepanenko, "New Developments in the Casimir Effect", Phys. Rep. 353, 1 (2001).
33. M. L.Roukes, Technical Digest of the 2000 Solid-State Sensor and Actuator Workshop, (Hilton Head Island, South Carolina, 2000).
34. R. S. Decca, D. López, E. Fischbach, and D. E. Krause, "Measurement of the Casimir Force Between Dissimilar Metals," Phys. Rev. Lett. 91 (2003), 050402.
35. D. López, R. S. Decca, E. Fischbach, and D. E. Krause, "MEMS Based Force Sensors: Design and Applications", Bell Labs Technical Journal 10 (2005), 61.
36. R. Decca. D. López, E. Fischbach, G. Klimchitskaya, D. Krause and V. Mostepanenko, "Precise Comparison of Theory and New Experiment for the Casimir Force Leads to Stronger Constraints on Thermal Quantum Effects and Long-range Interaction," Annals of Physics 318 (2005), 37.
37. The expression for the force is obtained through the derivative of the capacitance between a sphere and a plane. This capacitance is obtained in L Boyer, F Houzé, A Tonck, J-L Loubet and J-M Georges, "The Influence of Surface Roughness on the Capacitance between a Sphere and a plane", J. Phys. D: Appl. Phys. 27 (1994) 1504.
38. F. Chen, U. Mohideen, G. L. Klimchitskaya and V. M. Mostepanenko, "Experimental test for the conductivity properties from the Casimir force between metal and semiconductor" "Phys. Rev. A 74 (2006), 022103.

39. H.-C. Chiu, C.-C. Chang, R. Castillo-Garza, F. Chen, and U. Mohideen, "Experimental procedures for precision measurements of the Casimir force with an atomic force microscope", J. Phys. A: Math. Theor. 41 (2008), 164022.
40. W. J. Kim, M. Brown-Hayes, D. A. R. Dalvit, J. H. Brownell and R. Onofrio, "Anomalies in electrostatic calibrations for the measurement of the Casimir force in a sphere-plane geometry", Phys. Rev. A 78 (2008), 020101(R); Reply to "Comment on `Anomalies in electrostatic calibrations for the measurement of the Casimir force in a sphere-plane geometry'", Phys. Rev. A 79 (2009), 026102; R. S. Decca, E. Fischbach, G. L. Klimchitskaya, D. E. Krause, D. López, U. Mohideen, and V. M. Mostepanenko Comment on "Anomalies in electrostatic calibrations for the measurement of the Casimir force in a sphere-plane geometry", Phys. Rev. A 79 (2009), 026101.
41. Changhuei Yang, AdamWax, Ramachandra R. Dasari, and Michael S.Feld, "2p Ambiguity-Free Optical Distance Measurement with Subnanometer Precision with a Novel Phase-Crossing Low-Coherence Interferometer", Opt. Lett 27 (2002), 77.
42. R. S. Decca and D. López, "Measurement of the Casimir Force Using a Microelectromechanical Torsional Oscillator: Electrostatic Calibration", Int. J. Mod. Phys. A 24 (2009), 1748.
43. R. S. Decca, D. López, E. Fischbach, G. L. Klimchitskaya, D. E. Krause, and V. M. Mostepanenko, "Novel Constraints on Light Elementary Particles and Extra-Dimensional Physics from the Casimir Effect", Eur. Phys. J. C. 51 (2007), 963.
44. R. S. Decca, D. López, and E. Osquiguil, "New Results for the Casimir Interaction: Sample Characterization and Low Temperature Measurements", Proceedings of the "Quantum Field Theory under the Influence of External Conditions", Oklahoma, 2009, to be published.
45. E. D. Palik, editor, "Handbook of Optical Constants of Solids" (Academic Press, New York, (1995).
46. A. Lambrecht and S. Reynaud, "Casimir Force Between Metallic Mirrors", Eur. Phys. J. D 8 (2000), 309.
47. E. M. Lifshitz and L. P. Pitaevskii, Statistical Physics (Pergamon Press, Oxford, 1980) Pt.II.
48. R. S. Decca, D. López, E. Fischbach, G. L. Klimchitskaya, D. E. Krause, and V. M. Mostepanenko, "Tests of New Physics from Precise Measurements of the Casimir Pressure Between Two Gold-Coated Plates", Phys. Rev. D 75 (2007) 077101.
49. S. de Man et al., "No anomalous scaling in electrostatic calibrations for Casimir force measurements"; Phys. Rev. A 79, 024102 (2009).
50. C. Speake and C. Trenkel, "Forces between Conducting Surfaces due to Spatial Variations of Surface Potential"; Phys. Rev. Lett. 90, 160403 (2003)
51. W. J. Kim, A. O. Sushkov, D. A. R. Dalvit, and S. K. Lamoreaux, "Measurement of the Short-Range Attractive Force between Ge Plates Using a Torsion Balance", Phys. Rev. Lett. 103, 060401 (2009).
52. B.W. Hoogenboom et al., "A Fabry–Perot interferometer for micrometer-sized cantilevers"; Appl. Phys. Lett. 86, 074101 (2005).
53. O. Arcizet et al., "High-Sensitivity Optical Monitoring of a Micromechanical Resonator with a Quantum-Limited Optomechanical Sensor"; Phys. Rev. Lett. 97, 133601 (2006).

54. H. Miao, K. Srinivasan, and V. Aksyuk, "Integrated MEMS Tunable High Quality Factor Optical Cavity for Optomechanical Transduction," in Conference on Lasers and Electro-Optics, OSA Technical Digest (CD) (Optical Society of America, 2010), paper CPDA10.
55. T. J. Kippenberg and K. J. Vahala, “Cavity Optomechanics: Back-Action at the Mesoscale”, Science 29, Vol. 321, pp. 1172 – 1176 (2008).

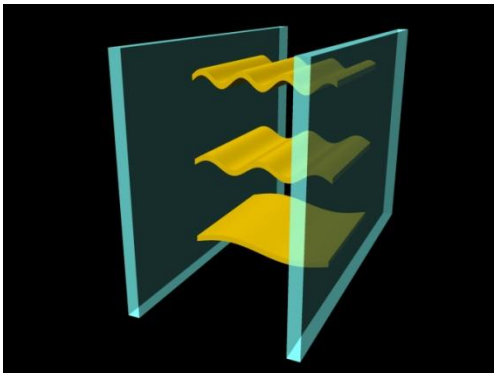

Figure 1. Schematic representation of the photonic modes confined between two metallic surfaces. The Casimir force between these two metallic surfaces arises due to the dependence of the energy spectrum of the confined electromagnetic modes on the separation between the surfaces.

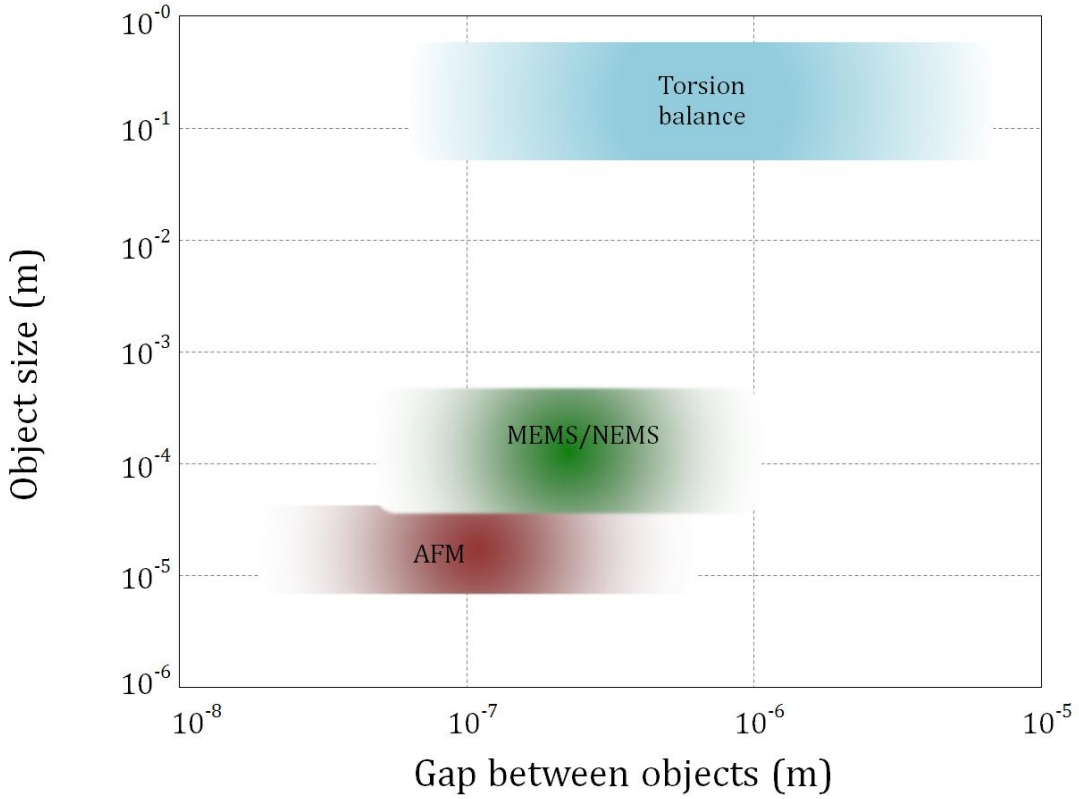

Figure 2. Comparison of the characteristic object's size and interaction range (gap) of experiments performed in the last decades to measure the Casimir force between bodies.

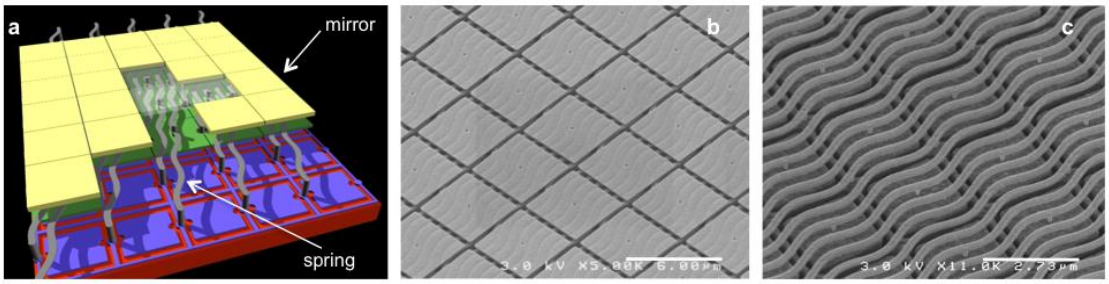

Figure 3. Ultra dense array of NEMS mirrors for maskless lithography: a) schematic representation of the array showing the mirror and spring layers and SEM images of the fabricated devices showing the mirrors array (b) and springs (c). Each mirror is 3 μm x 3 μm, the gap between them is around 100nm. In (c), the spring's width and spacing is also ≈ 100nm.

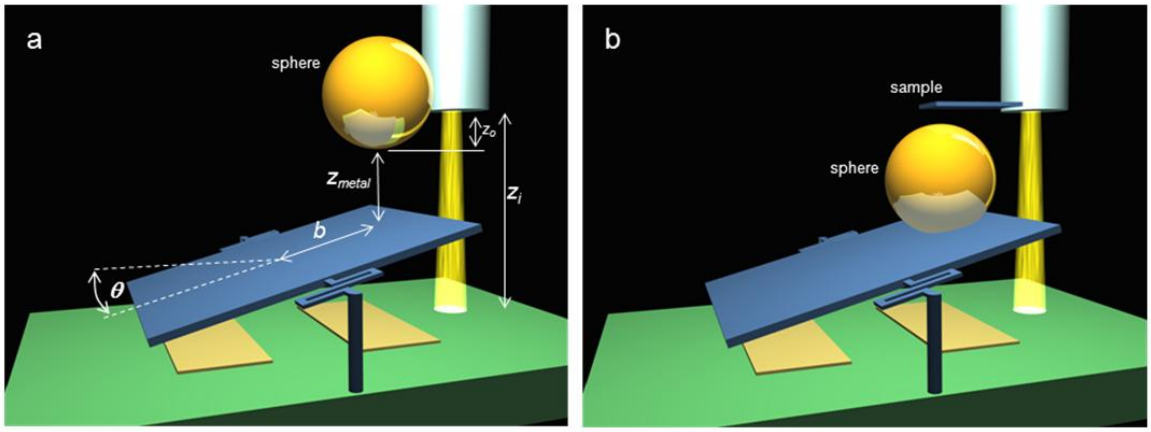

Figure 4: Schematic of the two configurations used for the experimental setup. a) sphere attached to the optical fiber. All the relevant dimensions are included. z_{metal} is the separation between the bodies, z_o is the distance between the end of the fiber and the end of the sphere, b is the lever arm, θ is the angular deviation of the oscillator, and z_g (not shown in the graph) is the distance between the top of the oscillator and the reference plate. b) Plate attached to the optical fiber assembly. All the dimensions have the same meaning, except for z_o which represents the distance between the end of the fiber and the bottom of the plate.

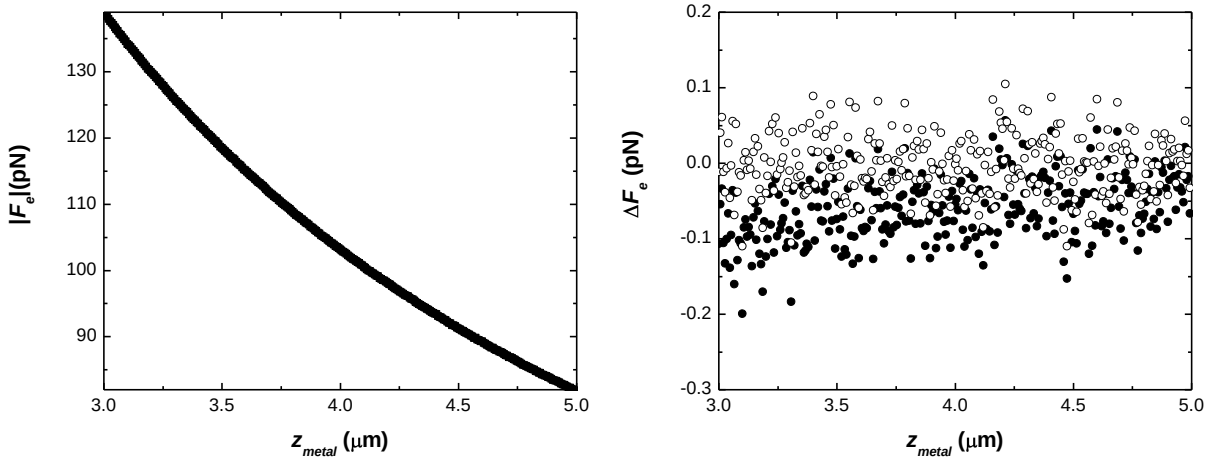

Figure 5: (a) Absolute value of the electrostatic force as a function of separation determined using the procedure described in the text and Eq. (6). (b) Difference between the measured values and Eq. (6) for

when either the best z_o (open circles) or $z_o^* = z_o + 1.5$ nm (full circles) are used in Eq. (6). Data shown was obtained for $(V_b - V_o) = 322.0$ mV.

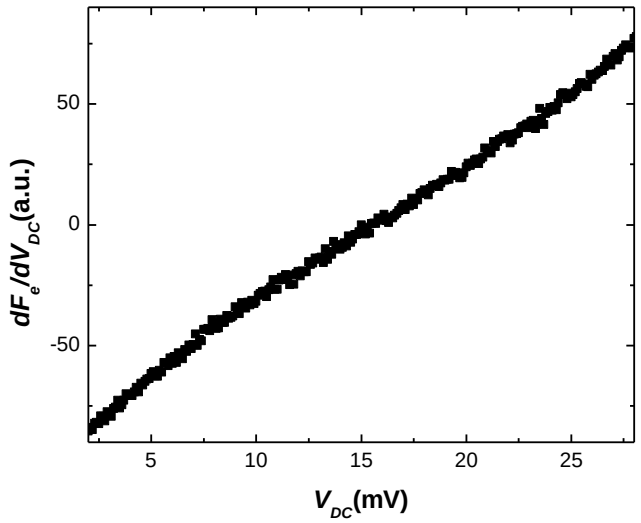

Figure 6: Magnitude of the derivative of the force $\partial F_e / \partial V_{DC}$ as a function of V_{DC}. The plot was obtained at $z_{metal} = 3.5$ μm when $V_{DC} = V_o$**.** Data do not fall in a straight line due to the increase of the electrostatic force (and θ) when $|V_{DC} - V_o|$ increases.

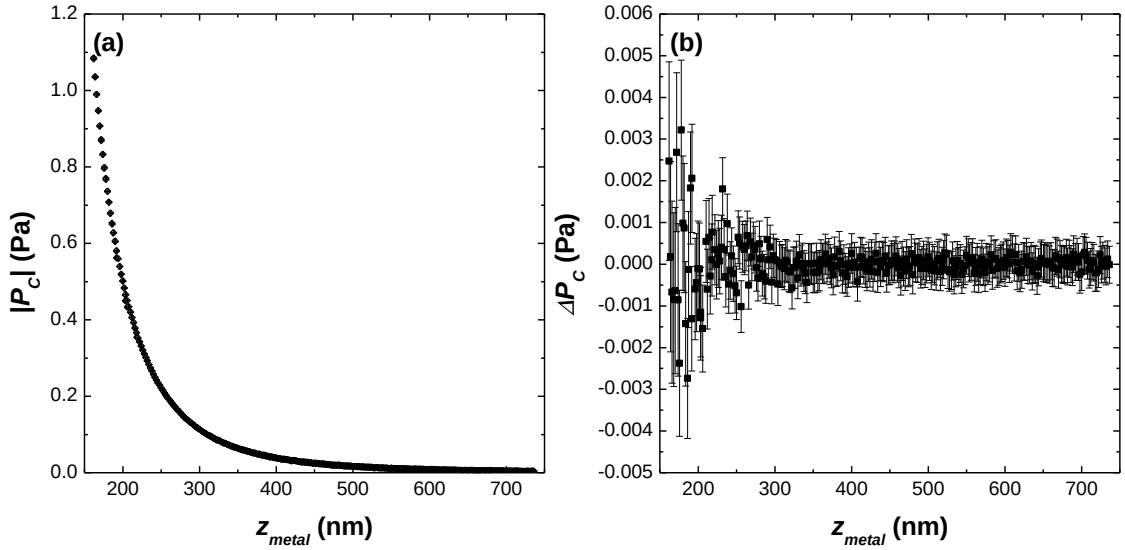

Figure 7: (a) Absolute value of the measured Casimir pressure as a function of separation for the setup from Fig. 4a, sample from Ref. [43] (open circles), and Fig. 4b, sample electrodeposited on a Si single crystal, Ref. [44] (closed circles). Both data sets are indistinguishable at this scale. (b) Difference between the data sets in (a). The difference was obtained at the separations measured in the newest sample. The pressure at these separations for the older sample was determined by linear interpolation. Error bars represent the 95% confidence level in both the separation and pressure determinations.

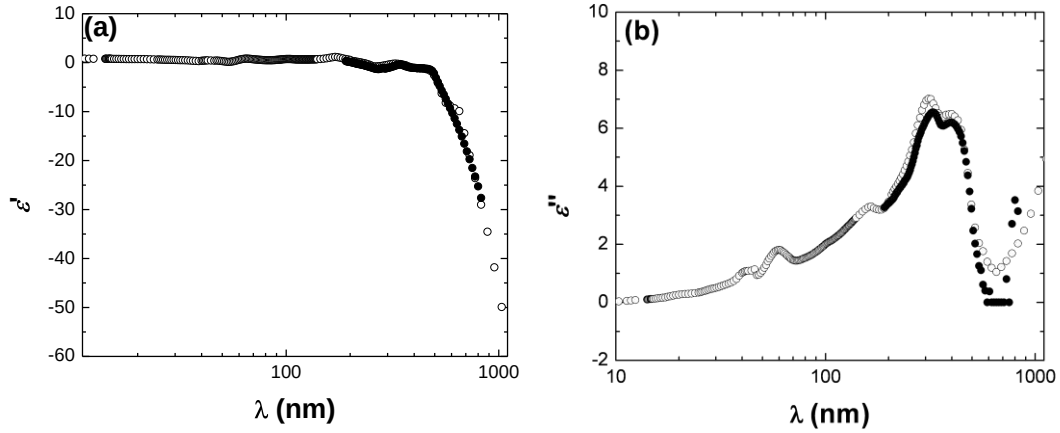

Figure 8: Filled circles show (a) ellipsometrically measured values of ε' and (b) ε'' as a function of wavelength. Tabulated data from Ref. [45] are displayed as open circles.

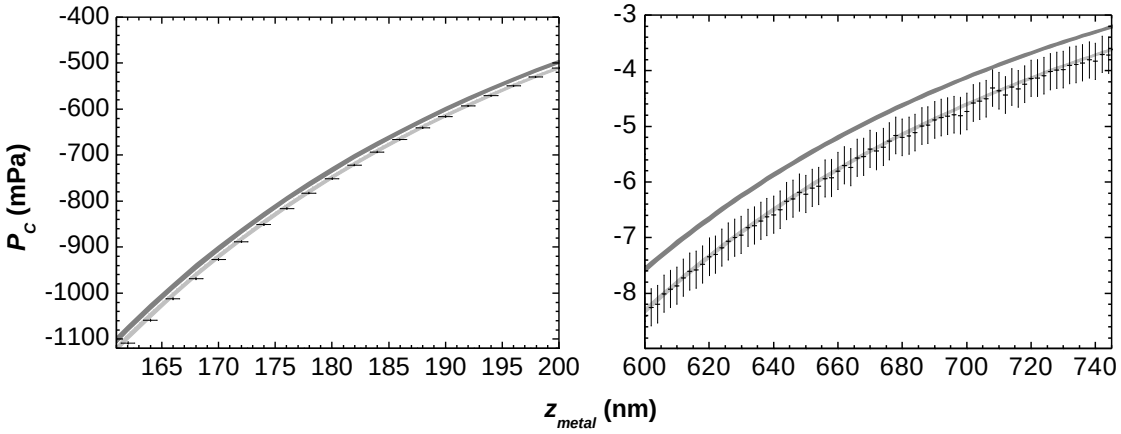

Figure 9: Measured and calculated Casimir pressure as a function of separation, for the closest (a) and furthest separations (b). The crosses represent the 95% confidence levels in the measured values. The dark gray band is the calculation (with the error represented by the thickness of the band) using the Drude model. The light gray is the same when the plasma model is used, see Ref. [48].

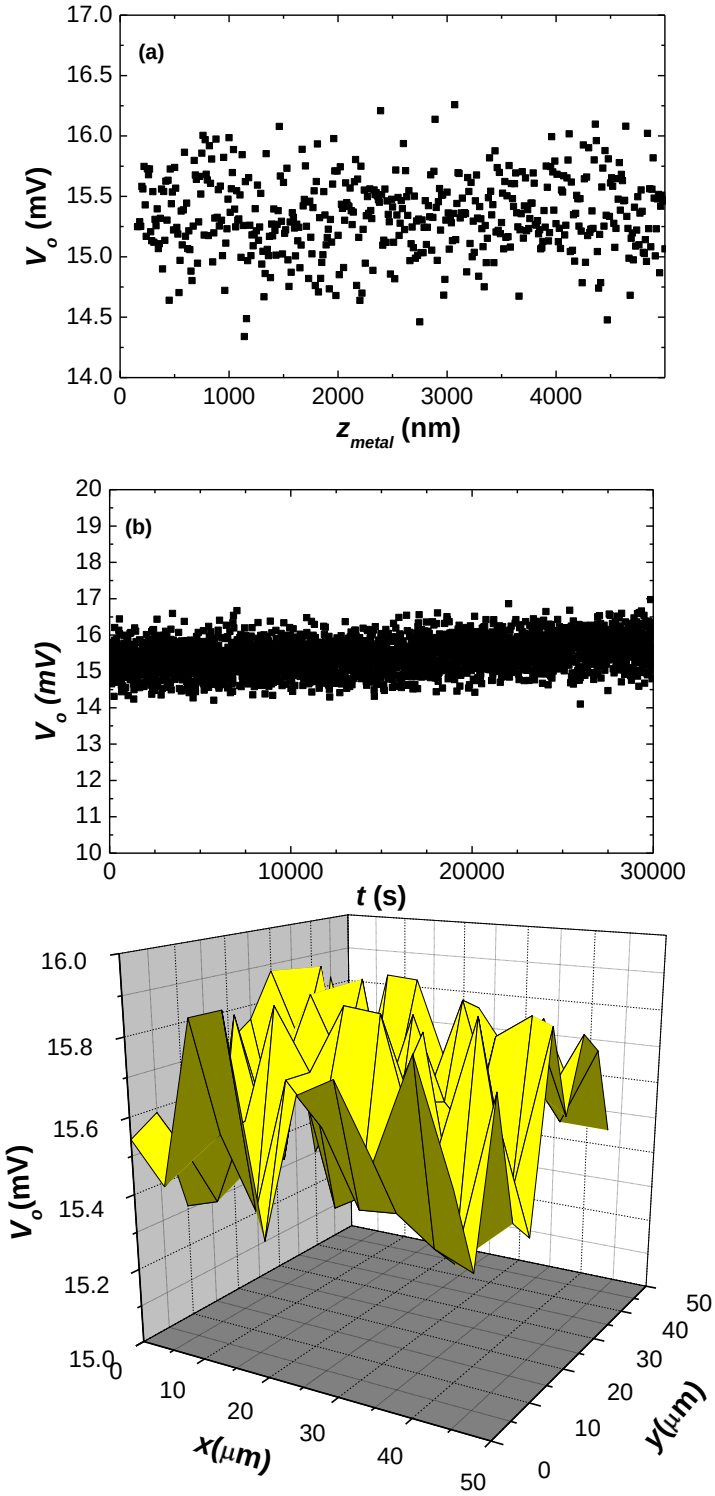

Figure 10 : Measurement of the residual potential V_o using the method shown in Fig. 3 as a function of (a) separation, (b) time, and (c) lateral position.

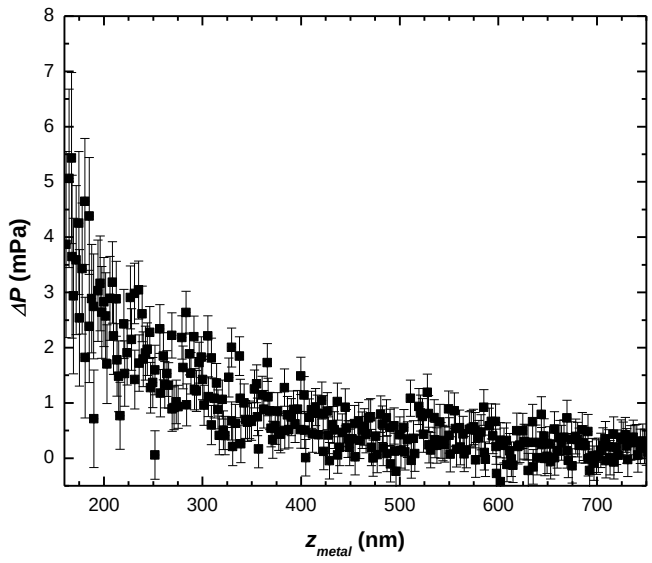

Figure 11: Difference between the determined Casimir pressure when the optimal V_b has been used and the determined pressure when $(V_b - V_o)$ = 5 mV has been used. The difference is well fitted by the electrostatic interaction. The error bars are obtained at the 95% confidence level.

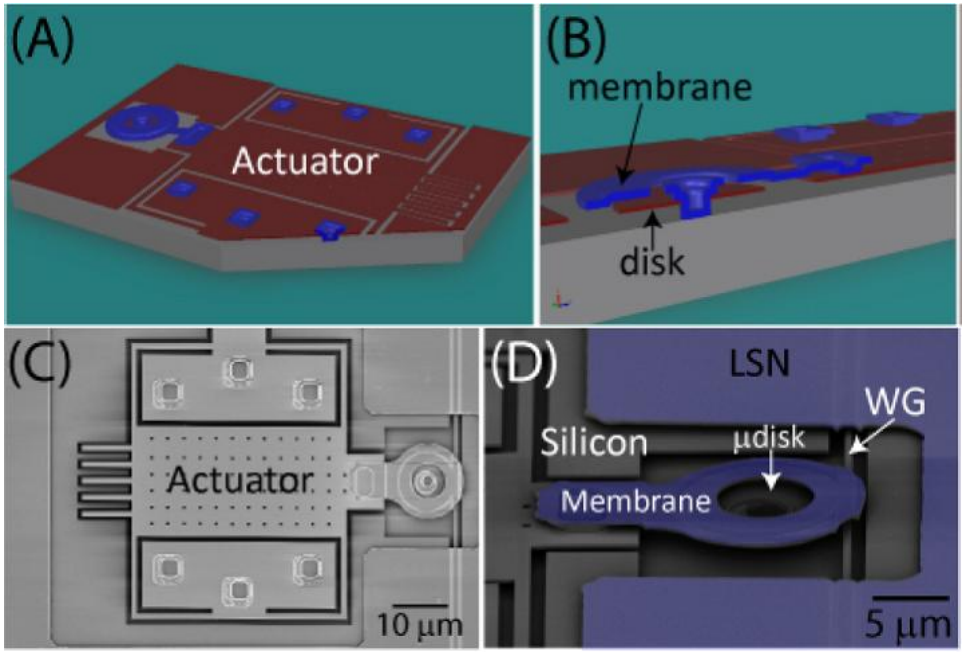

Figure 12: Schematic (A and B) and Scanning Electron Microscope images (C and D) of an integrated opto-mechanical transducer. Membrane is microfabricated from low stress silicon nitride (LSN). Actuator, microdisk optical resonator (μdisk), and waveguide (WG) are single crystal silicon.